3. Beamlines

In this section, we describe the activity status of the beamlines in FY2023, including frontend, optics and transport channel, radiation shielding of SPring-8, and SACLA beamlines. In addition to routine maintenance, several component upgrades and R&D were performed. Beamline upgrade and portfolio rearrangement are ongoing toward the SPring-8 major upgrade. Some beamline reconstructions were carried out during this period.

1. High heat load handling at X-ray beamlines

1-1. Liquid nitrogen supply system

The liquid nitrogen (LN2) circulation cooling system with a helium refrigerator, which is used to cool the first optical elements in almost all insertion device (ID) beamlines, consumes high maintenance costs, electricity, and cooling water. In addition, there is an urgent need for drastic aging measures after 20 years of operation. Therefore, we have been preparing LN2 supply facilities to provide LN2 directly to each beamline in the experimental hall. A new cooling system without the helium refrigerator was introduced, following the standard scheme of worldwide synchrotron radiation facilities.

The circulating LN2 for optics cooling at the beamline is cooled by heat exchange with LN2 continuously provided from the LN2 supply facility. In FY2022, four large cold evaporators (CEs) were installed outdoors on the inner side of each storage ring building (A, B, C, D), as shown in Fig. 1. In addition, vacuum-jacketed piping (VJP) was laid at the entrance between the CEs and the indoor interface point. In FY2023, 196 VJPs, each approximately 7.5 m long, were laid annularly on the ceiling of the storage ring tunnel (see Fig. 2), which is equipped with branches for each ID beamline, five LN2 collecting stations in the experimental hall, and six exhaust ports so that the nitrogen gas generated in the system could be transported to the existing experimental exhaust duct. To build a monitoring system for the CEs, wiring was installed to connect the external outputs of the pressure transmitter and liquid level gauge to the central monitoring room.

Fig. 1. LN2 cold evaporator (CE).

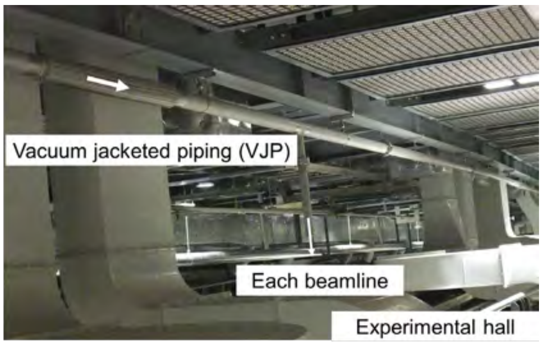

Fig. 2. VJPs for LN2 in experimental hall.

1-2. LN2-cooling double-crystal monochromator

On updating BL46XU, the first crystal in the double-crystal monochromator (DCM) was thickened to 70 mm from the original thickness of 35 mm to manage a greater heat load. The actuators in the fine Bragg rotation stages were exchanged to reduce vibration. In the commissioning of BL46XU, large vibration was detected in the DCM. The major vibration sources were the refrigerators of the LN2 circulator. The vibrations of the refrigerators propagated to the DCM along the LN2 transport pipes. The DCM vibration was reduced by placing weight on the LN2 transport pipes. The vibration in the DCM was changed from 180 nrad (before the reconstruction) to 88 nrad, as shown in Fig. 3.

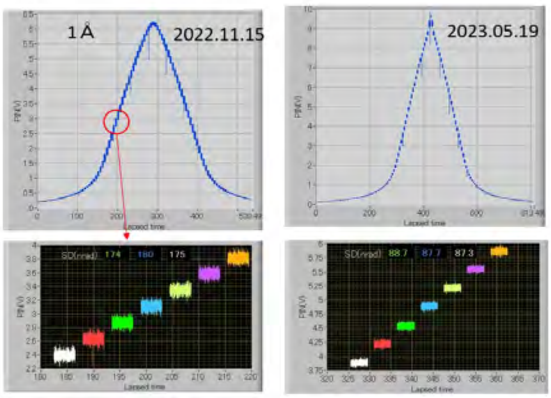

Fig. 3. Reduction of DCM vibration.

2. X-ray optics and beam transport

2-1. Commissioning of BL46XU

BL46XU was reconstructed as a beamline dedicated to HAXPES applications from December 2022 to March 2023. The main application targets are high-throughput HAXPES and ambient-pressure HAXPES. The optical components, shown in Fig. 4, were patterned after BL09XU, which was reconstructed for advanced HAXPES experiments in FY2021. The commissioning of the beamline optics was carried out in April and May 2023.

In the series of reconstruction, beryllium windows in the frontend section were removed to improve the beam uniformity. A set consisting of a differential vacuum pumping unit, a fast-closing valve, and a beam absorber was inserted to protect the vacuum of the storage ring from vacuum accidents at the beamline optics section. To further narrow the X-ray bandwidth, two sets of double channel-cut monochromators were installed. Silicon 220 reflection covers the X-ray energy range from 4.9 to 7.2 keV within a bandwidth of 300 meV, and 311 reflection covers 7.2 to 12.0 keV within the same bandwidth. As shown in Fig. 5, the inner reflection surfaces were processed by plasma etching to remove scratches, in collaboration with Osaka University [1]. An X-ray phase retarder shown in Fig. 6 was newly installed. Diamond plates were cut to reduce strain caused by clamping force. Monolithic Wolter type-I focusing mirrors were installed in both experimental hutches, EH1 and EH2, as shown in Fig. 7. The optical parameters of the mirror in EH1 are the same as those used in BL09XU EH1, that is, a working distance of 1.45 m and a magnification of 1/27. In contrast, the mirror in EH2 has a shorter working distance of 0.86 m and a smaller magnification of 1/50. Focusing sizes (vertical × horizontal) of 1 μm × 25 μm at EH1 and 0.7 μm × 14 μm at EH2 were achieved. The commissioning of the mirrors was completed, and the commissioning of the HAXPES stations with the mirrors began in May 2023.

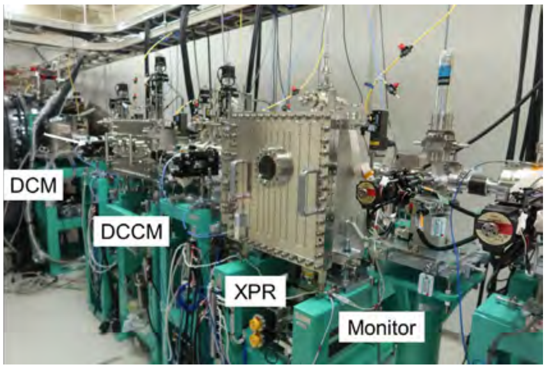

Fig. 4. Optical components in the optics hutch.

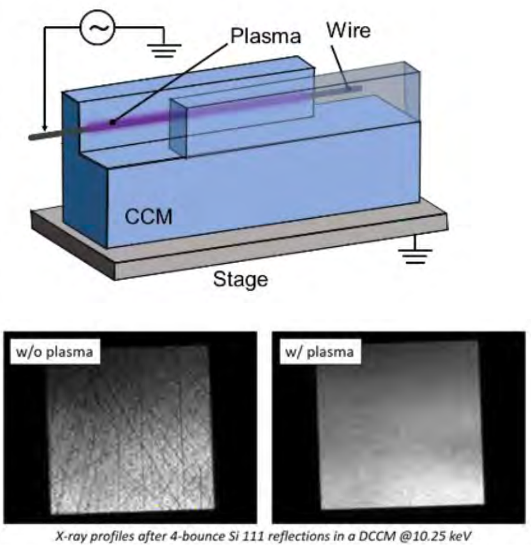

Fig. 5. Plasma etching of channel-cut crystal.

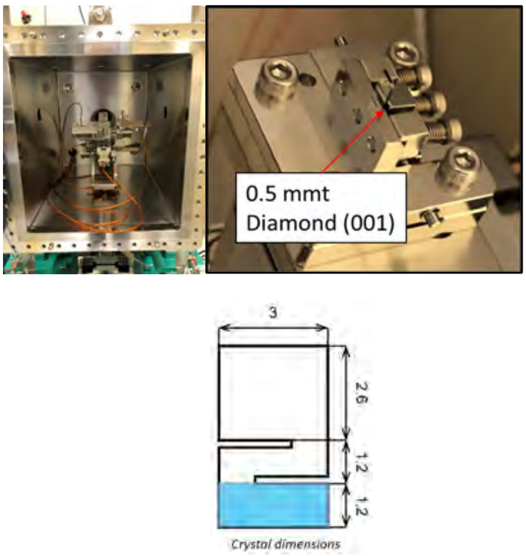

Fig. 6. X-ray phase retarder.

Fig. 7. Wolter mirror installed in EH1.

2-2. Upgrade of BL39XU

BL39XU is mainly dedicated to research fields of magnetism. To manage increasing user demands, the third experimental hutch 2 (EH2 in Fig. 8) was newly built, and the experimental apparatus was rearranged. As the common optical components, the optics hutch houses a DCM, newly developed harmonics-cut mirrors (see section 2-3), and an X-ray phase retarder, as shown in Fig. 9. In the new hutch, a monolithic Wolter mirror was newly designed to focus X-rays to an appropriate size. The reconstruction started in July 2023, and the commissioning has been continuing from January 2024.

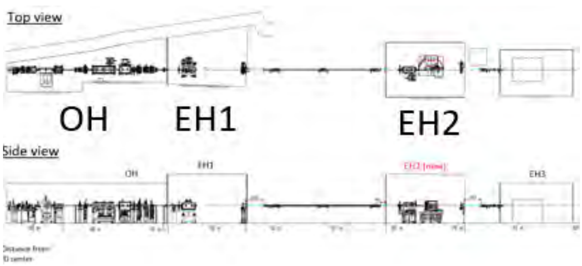

Fig. 8. Beamline design of upgraded BL39XU.

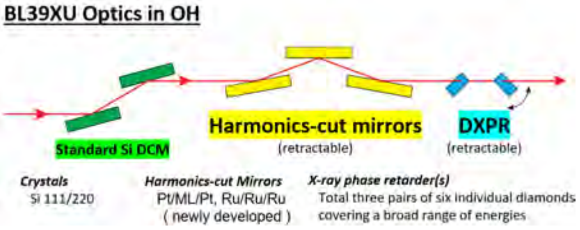

Fig. 9. Optical components in the optics hutch.

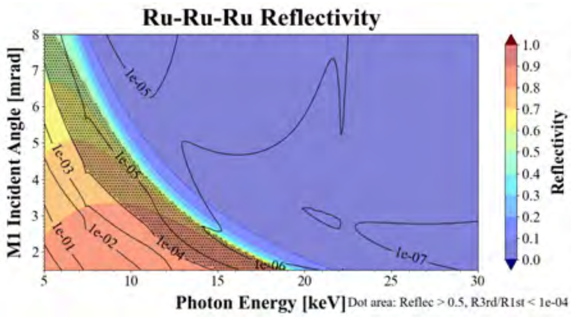

Fig. 11. Reflectivity of Ru-Ru-Ru mirror set.

2-3. Design of coaxial-exit higher-order cut mirror system for BL39XU

For higher purity of photon energy, a new higher-order cut mirror system was developed. It consists of three mirrors to achieve a coaxial exit, and the incident angle is selectable to cover a wide energy range. The configuration of the first and second mirrors mounted on a single stage enables the adjustment of incident angles with a reduced effect on the exit beam axis, as illustrated in Fig. 10. The third mirror is mounted on the position and rotation stages for fine adjustment of the exit beam axis. The typical reflectivity of the Ru-Ru-Ru mirror set is shown in Fig. 11.

This system was installed in the optics hutch at BL39XU, and the commissioning will be carried out in 2024A.

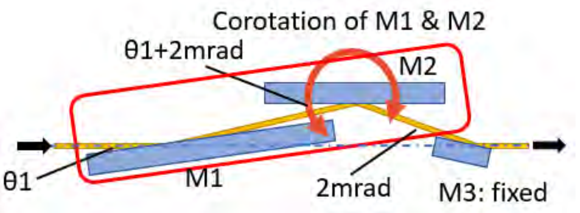

Fig. 10. Schematic view of coaxial-exit higher-order cut mirror system.

2-4. Upgrade and commissioning of BL07LSU

BL07LSU was reconstructed as an R&D beamline from April 2023. All gratings and mirrors were updated to the latest precision ones, and the monochromator type was changed to a collimated plane grating monochromator. In conjunction with the upgrade, vibration reduction techniques were used to achieve high energy resolution. The mechanics in the monochromator was redesigned to increase rigidity. Water pipe routing was optimized and low-vibration tubes (CFF4®) were adopted to reduce the effect of water flow. The commissioning and performance evaluation of the beamline were started in May 2023. The energy resolution was estimated to be 39,000 at 867 eV from the Ne resonant Auger spectrum, which is almost the same as the design value.

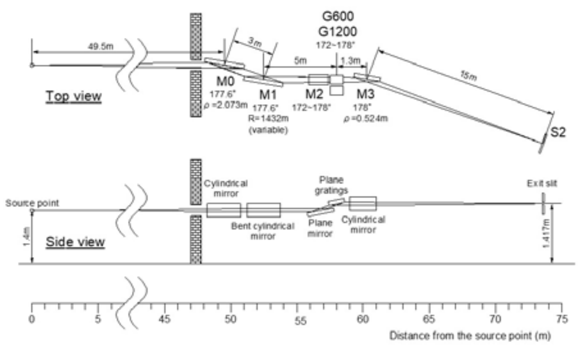

Fig. 12. Optical layout of upgraded BL07LSU.

2-5. Refurbishment of single multilayer monochromator in BL28B2

A single multilayer monochromator (SMM) was refurbished to facilitate the use of 25 keV and 40 keV at the sample position. The installation position was moved as far downstream as possible and the deflection direction was changed from downward to upward. Parameters of the multilayer mirror are shown in Table 1. A water-cooled filter was also installed upstream of the SMM to suppress unwanted total reflection components and heat load. Figure 13 shows the layout of these components. The commissioning will be started in April 2024. After a short commissioning period, the SMM will be opened for public use.

Table 1. Parameters of the multilayer mirror.

Multilayer	Materials	W/Si
	Period	5.3 nm on average (depth graded)
Substrate	Material	Si
	Size	L 1000 mm, W 60 mm, T 50 mm
	Effective length	980 mm
25 keV	Glancing angle	5.114 mrad
	Bandwidth	10%
	Reflectivity	87%
	Aperture	5.01 mm
40 keV	Glancing angle	3.194 mrad
	Bandwidth	10%
	Reflectivity	93%
	Aperture	3.13 mm

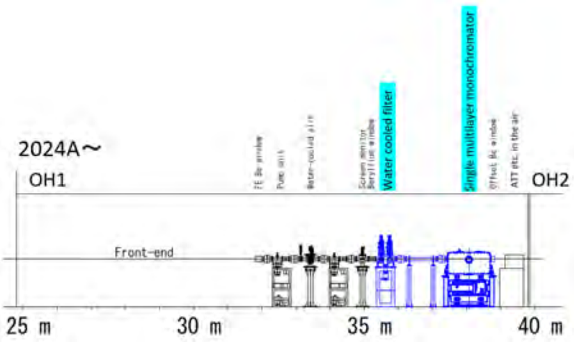

Fig. 13. Layout of the newly installed water-cooled filter and refurbished SMM at BL28B2 optics hutch 1 (OH1).

2-6. High-energy and high-flux beams using DMM

At BL05XU, high-flux X-rays at 100 keV from a double multilayer monochromator (DMM) are used for advanced X-ray analyses, including absorption imaging, Compton scattering imaging, diffraction imaging, and pair distribution function (PDF) analysis. 100 keV focusing beams with high flux [beam size: 0.3 μm (V) × 5 μm (H), flux: 1×10^{12} photons/s] and high resolution [beam size: 0.3 μm (V) × 0.3 μm (H), flux: 6×10^{10} photons/s] modes are also available [2]. To explore the potential of the undulator source in the higher energy region, we produced and evaluated X-ray beams at 130, 200, and 267 keV using the DMM. The DMM can monochromatize X-rays by adjusting the incident angle of the multilayers to satisfy the Bragg reflection condition for their wavelength. Table 2 summarizes the evaluated X-ray energy, energy bandwidth, photon flux, and other properties. Higher energy X-rays are expected to enable the observation of the internal structure of much larger and more complex objects using Compton scattering and diffraction imaging techniques. The penetrating power of heavy metals, such as lead, at 267 keV, is ten times higher than that at 100 keV. A high photon flux of over 1×10^{11} (photon/s) is available even at 267 keV, while the vertical beam size decreases with increasing X-ray energy due to the small spatial acceptance of the DMM under the small-incident-angle condition.

Table 2. Properties of high-energy beams produced using DMM.

X-ray energy (keV)	Energy bandwidth (%)	Beam size: (vertical) (mm). (FWHM)	Photon flux (photon/s)	Undulator gap (mm)
100	1.0	0.7	3×10^{13}	9.40
130	1.2	0.6	1×10^{13}	8.57
200	1.2	0.3	2×10^{12}	8.25
267	1.2	0.3	1×10^{11}	8.24

2-7. X-ray beam position monitor (XBPM)

We are progressively introducing an improved XBPM, in which four detector elements are arranged in an inclined position, to reduce the effect of changes in the filling pattern of the storage ring. The output signal from each blade detector element was systematically measured by varying the bias voltage of the photoelectron-collecting electrode and compared with that of the conventional XBPM, in which the detector elements are arranged in parallel. As a result, it was confirmed that a plateau region of the output signal can be formed with a bias voltage of +100 V or higher, even in the E-mode, where the effect of the filling pattern is most significant. In addition, an evaluation of the correction factor also confirmed that there are no changes that affect the output signal under conditions where a plateau region can be secured.

2-8. Energy-resolved beam monitoring system (ES-XBPM)

An energy-resolved beam monitoring system (ES-XBPM) for the X-ray beam exiting from the frontend ES-XBPM was developed at BL03XU, and in FY2023, the performance of this system was evaluated by scanning measurements with a high-energy-resolution SDD. When scanning the SDD with a pinhole attached to the light-receiving part, fluorescent X-rays from the pinhole material (tungsten) were generated as large noise, but this was successfully suppressed by making the pinhole double-structured with molybdenum based on particle and heavy ion transport code system (PHITS) simulations. This configuration enables accurate measurement of the light axis within a frontend slit (FES) aperture size of 1 mm × 1 mm. Furthermore, by using a similar technique to scan the FES in two dimensions with an aperture narrowed to 0.4 mm × 0.4 mm, we succeeded in acquiring highly energy resolved images using the SDD. The images revealed, for the first time, the shape of the undulator radiation over a wide area extending to a φ4 mm aperture in the preslit installed upstream of the FES. Although this approach does not extend to 2-D detectors in terms of real-time performance, it is noteworthy as a measurement method that provides valuable information that has never been available before.

3. Beamlines of SACLA

3-1. XFEL beamlines

The two XFEL beamlines (BL2 and BL3) have been stably operated in parallel throughout FY2023 to produce hard X-ray pulses. The main linac of SACLA has produced electron bunches at a 60 Hz repetition rate and delivered the electron beams to both beamlines on a pulse-by-pulse basis. In addition, the beam is also injected into the storage ring of SPring-8.

Even though the parallel operation of two XFEL beamlines started in 2017 and helped to increase the number of user experiments, it has been challenging sometimes when the photon energies differed largely between the two beamlines because there was a lack of capability to tune the beam envelope at the 60 Hz repetition rate. This limitation caused scheduling difficulties, particularly when one of the beamlines used very high or low photon energies. The pulsed quadrupole magnets were fully installed before the 2023B term to mitigate this situation. The beam parameters, such as the electron beam energy, peak current, and envelope, are now optimized independently for each pulse. The improvement has helped to remove the scheduling difficulties and allowed us to maximize the operation efficiencies.

There was also progress on the accelerator's automated tuning system with the adoption of machine learning technologies [3], and the system has been utilized to optimize X-ray parameters for user experiments. Recently, the X-ray spectral parameters, such as the central wavelength and the spectral brightness, can be optimized by monitoring the data from a high-resolution in-line spectrometer installed in FY2022. The spectrometer consists of a capillary filled with diamond microcrystals and offers a resolution of a few eV, providing detailed spectral shapes of every pulse. In 2023, the automated tuning system was successfully demonstrated to function stably to reduce the proportion of subpeaks and to narrow the spectral bandwidth of SASE beams in accordance with user requests.

XFEL beams are monochromatized by DCMs with silicon (111) crystals if needed. The system employs piezo stages for the precise adjustments of the height (ΔZ) and angle (Δθ) of the first crystal and also the tilt (Ty) of the second crystal. This year, a malfunction occurred in the stages for ΔZ and Ty of the DCM at BL2, and their control was lost. The issue was resolved by replacing a broken amplifier and updating the firmware of the piezo controller. The firmware will also be updated for the piezo controller of the DCM at BL3 to shorten the repair time in case a similar problem arises in the future.

3-2. Soft X-ray FEL beamline

The SACLA BL1 provides an intense soft X-ray pulse in the photon energy range from 40 to 150 eV. To provide the pulse-to-pulse spectral information in an almost nondestructive way, a quasi-in-line spectrometer (I-spec) has been developed. The single-shot spectral information is important from the viewpoint of data analysis of experiments and the consistent production of X-ray pulses.

The I-spec consists of a wavefront splitting system and a flat-field grazing-incidence spectrometer. A beam branching mirror, which is an elliptic cylindrical mirror with a sharp edge, picks up a small portion of an FEL beam and focuses the branched beam one-dimensionally onto the entrance slit of the spectrometer. The trend of the central photon energies observed with the I-spec has been compared with the measurement results obtained at EH4a. The results show reasonable agreement. The I-spec can also measure the spectra of the 3rd-order harmonics by using the 3rd-order diffraction of the grating. In the future, the single-shot spectral information will be utilized for the automated tuning of BL1 similarly to the XFEL beamlines.

TAKAHASHI Sunao[*1,2], OHASHI Haruhiko[*2], YAMAZAKI Hiroshi[*2], SENBA Yasunori[*2], YUMOTO Hirokatsu[*2], KOYAMA Takahisa[*2], INUBUSHI Yuichi[*3,4], MIYANISHI Kohei[*3], OWADA Shigeki[*3,4], YABUUCHI Toshinori[*3,4], TONO Kensuke[*3,4], and YABASHI Makina[*3,4]

[*1]Innovative Synchrotron Radiation Facility Division, RIKEN SPring-8 Center

[*2]Beamline Division, JASRI

[*3]Advanced Photon Technology Division, RIKEN SPring-8 Center

[*4]XFEL Utilization Division, JASRI

References:

[1] Hirano, T. et al. (2016). *Rev. Sci. Instrum.* **87**, 063118.

[2] Koyama, T. et al. (2024). *J. Synchrotron Rad.* **31** 276.

[3] Iwai, E. et al. (2023). *J. Synchrotron Rad.* **30**, 1048.